Design and Manufacturing of a Convergent-Divergent Test Section for Swirling Flow Apparatus

Alin BOSIOC[1], Romeo SUSAN-RESIGA[1], Sebastian MUNTEAN[2]

[(1)] National Center for Engineering of Systems with Complex Fluids, "Politehnica" University of Timişoara, Bd. Mihai Viteazul, 1, 300222, Timişoara, Romania

[(2)] Center for Advanced Research in Engineering Sciences, Romanian Academy – Timişoara Branch, Bd. Mihai Viteazul, 24, 300223, Timişoara, Romania

Abstract

The paper presents the hydrodynamic design and manufacturing of the test section for the swirling flow apparatus developed at the „Politehnica" University of Timisoara – National Center for Engineering of Systems with Complex Fluids.

The new test section provides a better visualization of the phenomenon, as well as the investigation of the velocity field using Laser Doppler Velocimetry. We present the design of the convergent part of the test section, for both the duct and nozzle shape. Preliminary LDV results for meridian and circumferential velocity profiles downstream the throat section are also shown.

Nomenclature

R_S	Upstream shroud radius
R_H	Upstream hub radius
R_P	Downstream pipe radius
R_*	Throat radius
L	Contraction length
z	Axial coordinate
$R_D(z)$	Convergent- divergent duct radius
$x \equiv z / R_*$	Dimensionless axial coordinate
$y \equiv R^2 / R_*^2$	Dimensionless cross section area
$X \equiv L / R_*$	Dimensionless contraction length
x_*	Axial throat position
$\tan\gamma_C$	Cone slope in the meridian half-plane
κ	Curvature in the meridian half-plane

Introduction

Experimental investigation of the precessing vortex rope in the draft tube of Francis turbines operated at partial discharge, [6], is usually performed on reduced scale models. However, the complexity of such experimental facilities, as well as the associated running costs, makes the basic hydrodynamic studies and flow control investigations difficult. As a result, simplified test facilities have been employed where the actual turbine model is replaced by a swirling flow generator, [4][8].

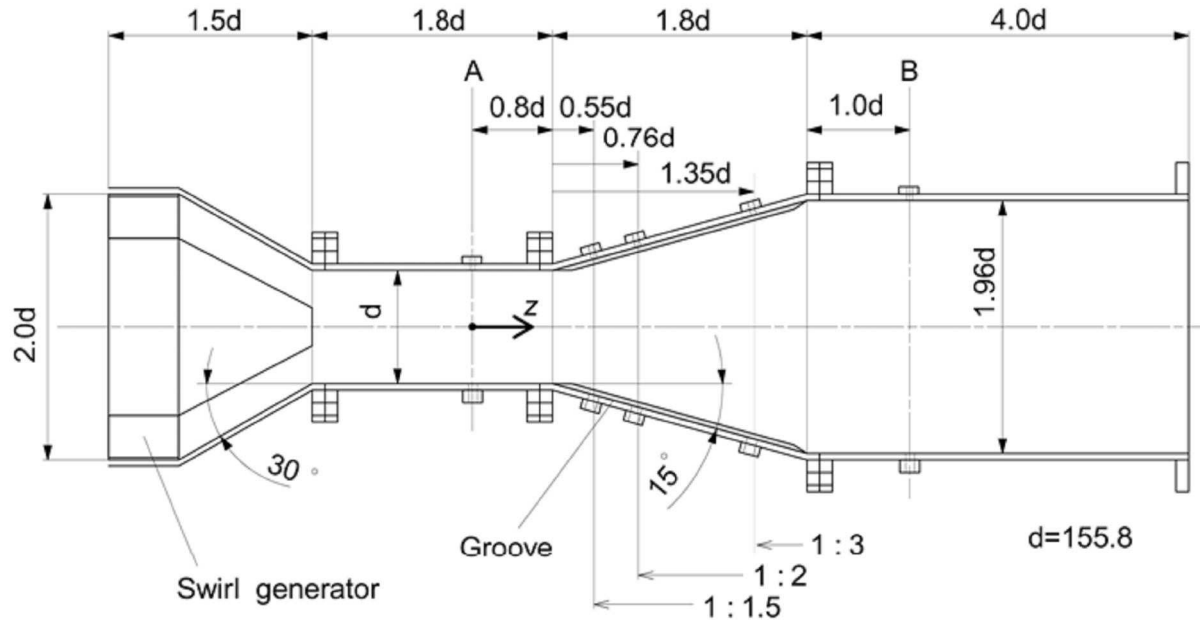

Fig. 1: Cross-section of the swirling flow apparatus developed by Kurokawa et al. [4].

Kurokawa et al. [4] studied the swirling flow in a conical diffuser using the apparatus shown in **Fig. 1**. They used an axial flow impeller, set at about $3.3d$ upstream the diffuser inlet, to produce a swirling flow. The pipe diameter upstream the conical diffuser is $d = 156mm$. A supplemental blower is arranged at far upstream of the divergent channel to change the flow rate widely. The conical diffuser is connected downstream to a straight pipe of the length $4.0d$. The diffuser angle is 30° and the inlet/outlet radius ratio is 1.96. In order to mitigate the self-induced instability of the swirling flow, Kurokawa et al. have tested various configurations of so-called "J-groove" (shallow grooves machined parallel to the pressure gradient) to control and suppress the swirl of the main flow. Their results showed that a significant reduction in the swirl strenght can be achieved with relatively small additional hydraulic losses created by the J-groove.

Susan-Resiga et al. [8] developed a swirling flow apparatus included in a closed-loop hydraulic circuit, with the possibility of producing a cavitating vortex rope similar to the phenomenon encounted in Francis turbines at part load. In addition, this test rig allows the evaluation of the jet control technique for stabilizing the decelerated

swirling flows. The initial design of the swirl apparatus presented in [8] uses a convergent-divergent test section inspired from Kurokawa et al. [4], with fixed guide vanes for generating the swirling flow. Preliminary investigations reveal that this configuration does not produce the desired spiral vortex breakdown, although a form of vortex breakdown and associated pressure fluctuations are present in the conical part of the test section. As a result, we have proceeded with a systematic design and analysis of both the swirl generator as well as the test section, in order to obtain a swirling flow apparatus capable of reproducing the actual phenomenon encountered in the draft tube cone of Francis turbines operated at part load.

This paper presents the hydrodynamic design of the convergent-divergent test section of the swirling flow apparatus, as well as the experimental setup for LDV investigations of the velocity field.

Duct Convergent Section

The convergent part of the convergent-divergent duct insures a smooth transition from the upstream pipe of radius R_S to the conical part of the duct. Before merging with the cone, the convergent part reaches a minimum radius at the throat, R_*. The throat radius is considered here as reference length in order to make all lengths dimensionless. At the beginning of the convergent part, the duct radius $R_D(z)$ must have vanishing first and second order derivatives in order to smoothly merge with the upstream pipe. At the end of the convergent part, the first derivative should correspond to the cone slope, while the second derivative vanishes. These geometrical conditions can be written as follows for the convergent part of the duct:

$$R_D(0) = R_S\,, \tag{1}$$

$$\frac{dR_D}{dz}(0) = 0\,, \tag{2}$$

$$\frac{d^2R_D}{dz^2}(0) = 0\,, \tag{3}$$

$$\frac{dR_D}{dz}(L) = \tan\gamma_C\,, \tag{4}$$

$$\frac{d^2R_D}{dz^2}(L) = 0\,. \tag{5}$$

$$\min_{z=0\ldots L} R_D(z) = R_*\,. \tag{6}$$

Since there are six conditions for the convergent duct shape, a fifth order polynomial might be used for $R_D(z)$, with coefficients determined from (1)...(6). However, following the procedures used to design the contractions of wind tunnels, [1], we are

going to determine the dimensionless cross-section variation $y_D(x)$, $x = 0...X$ rather than the radius variation $R_D(z)$. Expressing the first and second order derivatives of the radius in the new dimensionless variables,

$$\frac{dR}{dz} = \frac{1}{2\sqrt{y}}\frac{dy}{dx}, \tag{7}$$

$$R_* \frac{d^2R}{dz^2} = \frac{1}{2\sqrt{y}}\left[\frac{d^2y}{dx^2} - \frac{1}{2y}\left(\frac{dy}{dx}\right)^2\right], \tag{8}$$

we can translate the conditions (1)…(6) into the corresponding form for $y_D(x)$. However, the condition (6) cannot be directly enforced since the $\min_{z=0...L} R_D(z)$ is not apriori known. As a result, we define the following set of conditions,

$$y_D(0) = y_D^{(1)} \equiv R_S^2 / R_*^2, \tag{9}$$

$$\frac{dy_D}{dx}(0) = 0, \tag{10}$$

$$\frac{d^2y_D}{dz^2}(0) = 0, \tag{11}$$

$$y_D(X) = y_D^{(2)}, \tag{12}$$

$$\frac{dy_D}{dx}(X) = 2\sqrt{y_D^{(2)}}\tan\gamma_C, \tag{13}$$

$$\frac{d^2y_D}{dx^2}(X) = 2\tan^2\gamma_C, \tag{14}$$

where $y_D^{(2)}$ is going to be iteratively adjusted in order to satisfy (6). Assuming a fifth order polynomial,

$$y_D(x) = a_0 + a_1x + a_2x^2 + a_3x^3 + a_4x^4 + a_5x^5, \tag{15}$$

conditions (9), (10) and (11) immediately give $a_0 = y_D^{(1)}$ and $a_1 = a_2 = 0$. The remaining three conditions, (12), (13) and (14) lead to the following system of linear equations:

$$a_3 + Xa_4 + X^2a_5 = \left(y_D^{(2)} - y_D^{(1)}\right)/X^3 \equiv b_1, \tag{16}$$

$$3a_3 + 4Xa_4 + 5X^2a_5 = \left(2\sqrt{y_D^{(2)}}\tan\gamma_c\right)/X^2 \equiv b_2, \tag{17}$$

$$3a_3 + 6Xa_4 + 10X^2a_5 = \tan^2\gamma_c / X \equiv b_3, \tag{18}$$

The solution of system of equations (16), (17), (18) is

$$a_3 = 10b_1 - 4b_2 + b_3\,, \tag{19}$$

$$a_4 = \left(-15b_1 + 7b_2 - 2b_3\right)/\,X\,, \tag{20}$$

$$a_5 = \left(6b_1 - 3b_2 + b_3\right)/\,X^2\,, \tag{21}$$

In order to satisfy (6) we must find the throat location by finding the minimum value of $y_D(x)$. First we find the throat location x_* by cancelling the first derivative

$$\begin{aligned} &\frac{dy}{dx}(x_*) = 0 = x_*^2\left(3a_3 + 4a_4 x_* + 5a_5 x_*^2\right) \\ &\Rightarrow\; x_* = \frac{-2a_4 + \sqrt{4a_4^2 - 15a_3 a_5}}{5a_5} \end{aligned}\,, \tag{22}$$

then we insert the above value of x_* into (15) to find $y_D(x_*)$. The value $y_D^{(2)}$ is iteratively corrected until $y_D(x_*) = 1$.

Let us present an example of convergent duct. Choosing an upstream radius $R_S = 1.5R_*$ gives $y_D^{(1)} = 2.25$. We choose a cone angle, $\gamma_C = 8.5^\circ$, within the normal range for the discharge cones of hydraulic turbines. The total length of the convergent part of the duct is a design parameter. In our case, we choose $L = 2R_*$, or in dimensionless form $X = 2.0$, based on the throat curvature criteria presented below. The condition $y_D(x_*) = 1$ is satisfied at $x_* = 1.741362$, with a corresponding value $y_D^{(2)} = 1.050430$, resulting in the duct shape shown **Fig. 2**. The polynomial coefficients are $a_3 = -1.794641$, $a_4 = 1.381482$ and $a_5 = -0.2795673$.

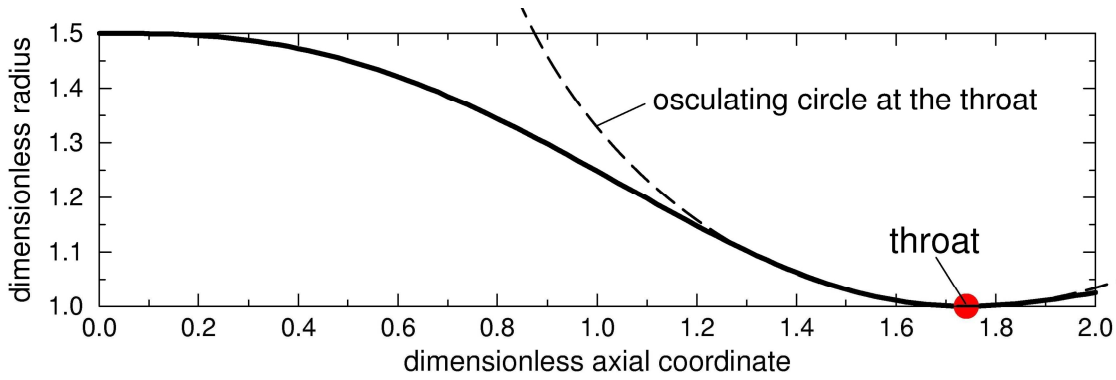

Fig. 2: Duct shape in the convergent part

If $y_D^{(1)}$ and γ_C are parameters specific to the test rig, the dimensionless length of the convergent part X is a design parameter. One possible criterion for choosing X is related to the duct surface curvature at the throat. The curvature at the throat is given by the reciprocal of the throat radius R_* in a plane normal to the symmetry axis and

by the reciprocal of the osculating circle radius, shown with dashed line in **Fig. 2**, in the meridian plane. The duct surface at the throat has a saddle shape, since one curvature is positive while the other is negative. From the hydrodynamic point of view, it is convenient to have equal curvature in both planes, meaning that the radius of the osculating circle from **Fig. 2** should be equal to the throat radius R_*. This condition leads to the dimensionless length X. In general, given the duct shape $R_D(z)$ we can compute the curvature in the meridian half-plane as [5]

$$\kappa_D(z)=\frac{\dfrac{d^2R_D}{dz^2}}{\left[1+\left(\dfrac{dR_D}{dz}\right)^2\right]^{3/2}}, \tag{23}$$

Using Eqs. (7) and (8) the dimensionless curvature can be written as

$$R_*\kappa_D(x)=\frac{\dfrac{1}{2\sqrt{y_D}}\left[\dfrac{d^2y_D}{dx^2}-\dfrac{1}{2y_D}\left(\dfrac{dy_D}{dx}\right)^2\right]}{\left[1+\dfrac{1}{4y_D}\left(\dfrac{dy_D}{dx}\right)^2\right]^{3/2}}, \tag{24}$$

With $X=2.0$, as chosen in the above example, we have $R_*\kappa_D(x_*)=0.999711$. Obviously, the radius of curvature in the meridian half-plane, at the throat, increases with the length X, thus decreasing the corresponding meridian curvature.

Central Body Shape

We turn our focus now to the central body, more precisely on the conical shape ending the upstream hub up to the throat section. The annular upstream cross-section is bound by the outer radius R_S and inner radius R_H. Since the average discharge velocity should increase in the convergent region, we obviously should have $R_S^2-R_H^2>R_*^2$, i.e. the upstream cross-section area should be larger than the throat area. We will call “nozzle” the conical transition from the radius R_H to vanishing radius at the throat, since for our swirl apparatus this will be used also to inject the control jet along the symmetry axis. As a result, we have to design the nozzle shape $R_N(z)$, $z=0...z_*$, with $R_N(0)=R_H$ and $R_N(z_*)=0$.

Since we have already designed the duct shape, the nozzle shape should result once an area variation is assumed from upstream to the throat. A cross-section variation commonly employed for wind tunnels is

$$AR(x) = AR_0 \left\{ \left[-10\left(\frac{x}{x_*}\right)^3 + 15\left(\frac{x}{x_*}\right)^4 - 6\left(\frac{x}{x_*}\right)^5 \right] \left[1 - \frac{1}{AR_0} \right] + 1 \right\}, \tag{25}$$

where the inlet-throat area ratio is $AR_0 = \left(R_S^2 - R_H^2 \right) / R_*^2$. This fifth order polynomial introduced by Bell and Mehta has been modified by Brassard and Ferchichi [2] by introducing an additional parameter n,

$$AR(x) = AR_0 \left\{ \left[-10\left(\frac{x}{x_*}\right)^3 + 15\left(\frac{x}{x_*}\right)^4 - 6\left(\frac{x}{x_*}\right)^5 \right] \left[1 - \frac{1}{AR_0^{1/n}} \right] + 1 \right\}^n, \tag{26}$$

The exponent n can be a function of $\left(x / x_* \right)$, eventually. In our case we will use the parameter n in order to optimize the nozzle shape [5].

On the other hand, the area of the cross-section between nozzle and duct can be approximated by a cone segment, with the cone generating line alingned with the normal direction to the duct,

$$A(z) = \pi \left(R_D^2(z) - R_N^2(z) \right) \sqrt{1 + \tan^2 \gamma_D(z)}, \tag{27}$$

where $\tan\gamma_D$ is the current slope of the duct, given by (7). The dimensionless area ratio will be:

$$AR(x) = \left(y_D(x) - y_N(x) \right) \sqrt{1 + \tan^2 \gamma_D(x)}, \tag{28}$$

As a result, the following parametric representation of the needle is obtained:

$$y_N(x) = y_D(x) - AR(x) / \sqrt{1 + \tan^2 \gamma_D(x)}, \tag{29}$$

$$x_N(x) = x + \left(\sqrt{y_D(x)} - \sqrt{y_N(x)} \right) \tan \gamma_D(x), \tag{30}$$

Note that in Eqs.(29) and (30) the cross-section is considered normal to the duct surface only, through $\tan\gamma_D$, therefore in general it is not normal to the nozzle surface. However, the above approximation is quite acceptable for design purposes.

When using the area ratio variation $AR(x)$ given by Eq. (26) to compute the nozzle shape with Eqs. (29) and (30), the result depends on the exponent n for a given upstream-throat area ratio AR_0. As a result, we should address the issue of finding the optimum value for n, by examining either the slope (31) or the curvature (32) of the nozzle in the meridian half-plane.

$$\tan \gamma_N = \frac{dR_N / dz}{dz_N / dz} = \frac{d\sqrt{y_N(x)} / dx}{dx_N / dx}, \tag{31}$$

$$\kappa_N(z)=\frac{\dfrac{d^2R_N(z)}{dz^2}\dfrac{dz_N(z)}{dz}-\dfrac{dR_N(z)}{dz}\dfrac{d^2z_N(z)}{dz^2}}{\left[\left(\dfrac{dz_N(z)}{dz}\right)^2+\left(\dfrac{dR_N(z)}{dz}\right)^2\right]^{3/2}}$$

$$R_*\kappa_N(x)=\frac{\dfrac{d^2\sqrt{y_N(x)}}{dx^2}\dfrac{dx_N(x)}{dx}-\dfrac{d\sqrt{y_N(x)}}{dx}\dfrac{d^2x_N(x)}{dx^2}}{\left[\left(\dfrac{dx_N(x)}{dx}\right)^2+\left(\dfrac{d\sqrt{y_N(x)}}{dx}\right)^2\right]^{3/2}}, \tag{32}$$

As a design example, we consider a hub radius $R_H=0.9R_*$, or $R_H/R_S=3/5$. The corresponding inlet-throat area ratio is $AR_0=1.5^2-0.9^2=1.44$. **Fig. 3** shows with dashed lines the shape, slope and curvature of the nozzle for the implicit value of $n=1$ in Eq. (26). One can see that the slope increases in magnitude as we approach the throat, reaches a maximum (negative) value, then it decreases where the curvature is positive with a dimensionless value larger than 0.2. However, we would prefer that the maximum slope of the needle be as small as possible in order to avoid or delay flow detachment. When optimizing the value of n according to this criterion, we find $n=0.21$, with corresponding nozzle shape, slope and curvature shown with solid lines in **Fig. 3**. For the downstream half of the nozzle the slope has little variation and very small curvature, resulting practically in a conical shape, with cone half-angle of $33^\circ\pm1.5^\circ$.

The optimized shape of the converging part of the swirl apparatus is shown in **Fig. 4**. The dashed lines show several cross-sections used to compute the nozzle shape from a given duct shape and an area ratio variation.

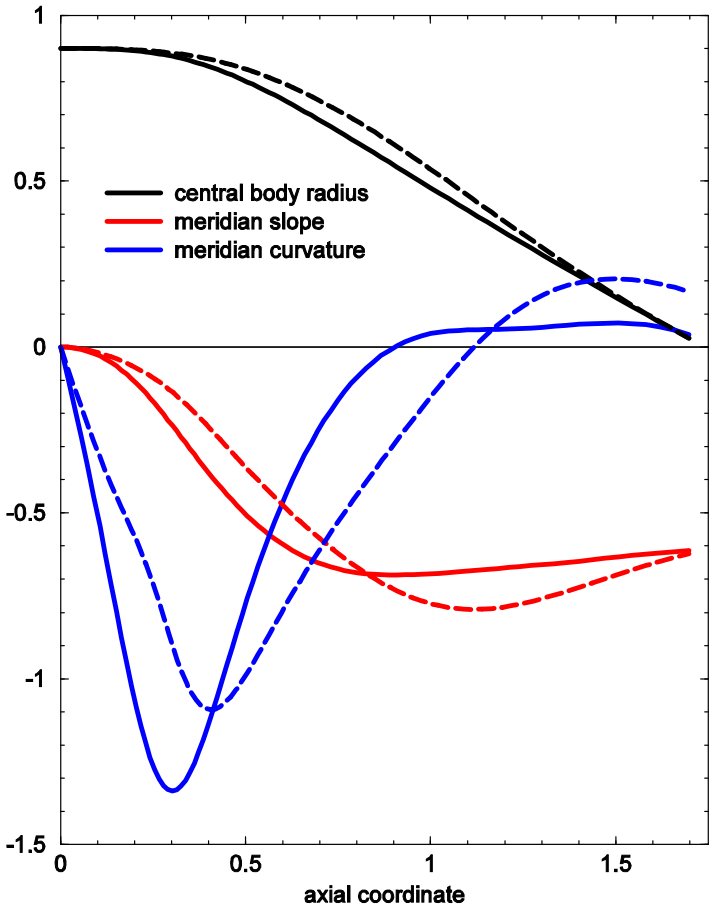

Fig. 3: Nozzle shape, slope and curvature for implicit value $n=1$ (dashed lines) and optimized value $n=0.21$ (solid lines) .

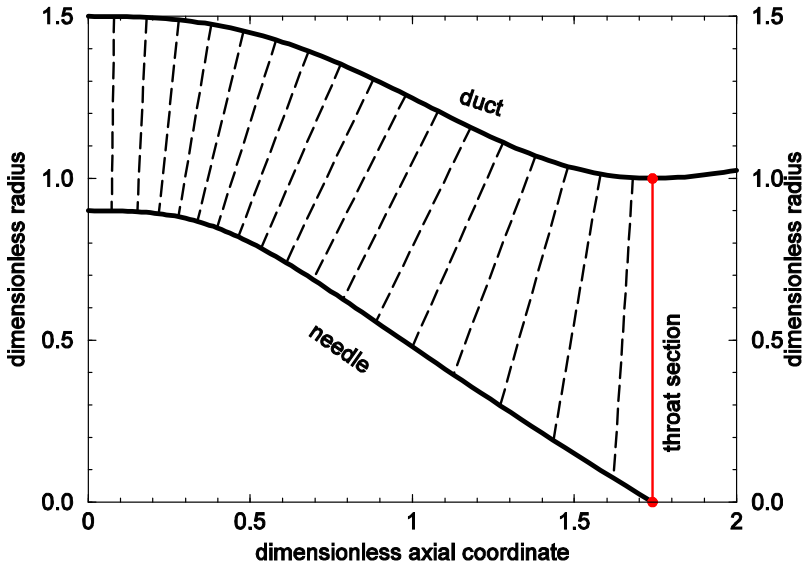

Fig. 4: Converging part of the swirl apparatus test section: duct upstream radius $1.5R_*$, nozzle uspstream radius $0.9R_*$, throat radius R_*, throat location $x_* = 1.741362R_*$, overall area contraction ratio 1.44.

Technological approximation of the duct and nozzle shape

In order to manufacture the convergent part of the duct, and the nozzle, respectively, the curves shown in **Fig. 4** and **Fig. 5** should be approximated with piecewise circular arcs. This is equivalent with a piecewise constant approximation of the curvature.

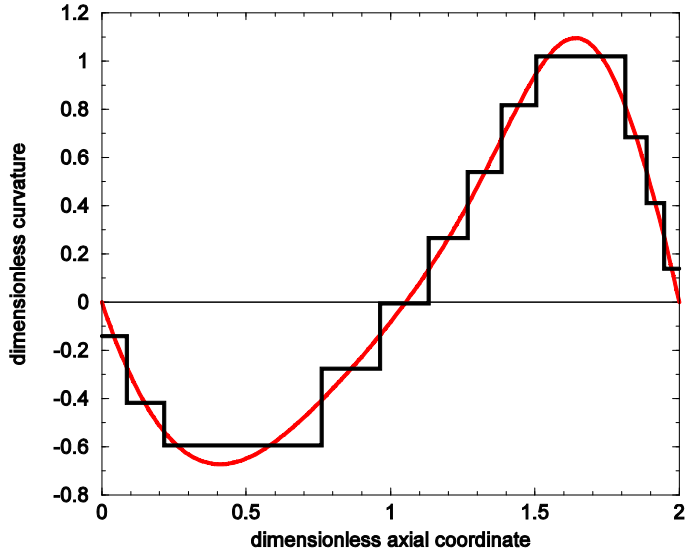

Fig. 5: Piecewise constant approximation of the convergent duct curvature, Eq.(24).

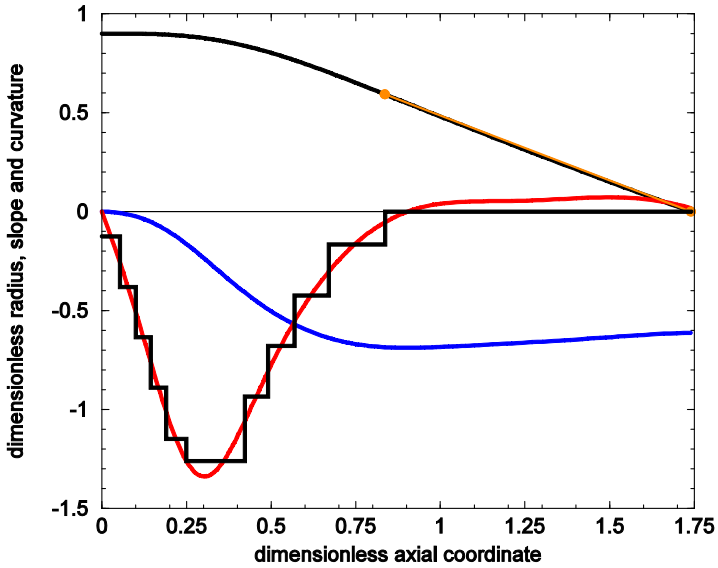

Fig. 6: Piecewise constant approximation of nozzle curvature, Eq.(32).

The actual approximation by circular arcs used for manufacturing is presented in Table 1 and Table 2, for the duct and nozzle, respectively. Each circular arc is given by its end points and radius. Note that the piecewise constant approximation of the curvature, **Fig. 5** and **Fig. 6** was built such that the approximation error is bounded by a given value for all intervals.

Table 1. Coordinates for manufacturing the duct

z1 [mm]	r1 [mm]	z2 [mm]	r2 [mm]	radius [mm]
.0000000	75.00000	4.319993	74.98197	-353.0315
4.319993	74.98197	10.82779	74.74422	-119.7979
10.82779	74.74422	38.03905	68.03133	-84.23337
38.03905	68.03133	48.19839	63.29736	-181.6042
48.19839	63.29736	56.60459	59.06429	line
56.60459	59.06429	63.38782	55.81990	187.8664
63.38782	55.81990	69.21248	53.41444	92.65956
69.21248	53.41444	75.19407	51.52172	61.23537
75.19407	51.52172	90.64444	50.12074	49.05071
90.64444	50.12074	94.32696	50.46144	73.11180
94.32696	50.46144	97.35147	50.85618	121.7277

Table 2. Coordinates for manufacturing the central body

z1 [mm]	r1 [mm]	z2 [mm]	r2 [mm]	radius [mm]
.0000000	45.00000	2.659301	44.99425	-397.0426
2.659301	44.99425	5.016300	44.96014	-131.6174
5.016300	44.96014	7.228743	44.87730	-78.85811
7.228743	44.87730	9.505363	44.71393	-56.26193
9.505363	44.71393	12.46856	44.33909	-43.56896
12.46856	44.33909	21.12106	41.86760	-39.66452
21.12106	41.86760	24.56620	40.30884	-53.56505
24.56620	40.30884	28.46138	38.23031	-73.77153
28.46138	38.23031	33.53770	35.14875	-118.1273
33.53770	35.14875	41.82926	29.61700	-301.0559
41.82926	29.61700	87.00000	0.00000	line

Test Section Design and Manufacturing

The shape of the meridian cross-section of the swirling flow apparatus is shown in **Fig. 7**, where both the convergent and divergent parts of the duct are assembled. The conical diffuser has a half angle of $\gamma_C = 8.5^\circ$, and the outlet diameter of $160\,mm$. The outlet/inlet area ratio of the diffuser is 2.56. This is the shape of the computational domain used for the 2D axi-symmetric turbulent swirling flow simulations.

Fig. 7: Test section of the swirling flow apparatus, in a meridian half-plane.

The duct is made from transparent plexiglass, in order to allow flow visualization and velocity measurements.

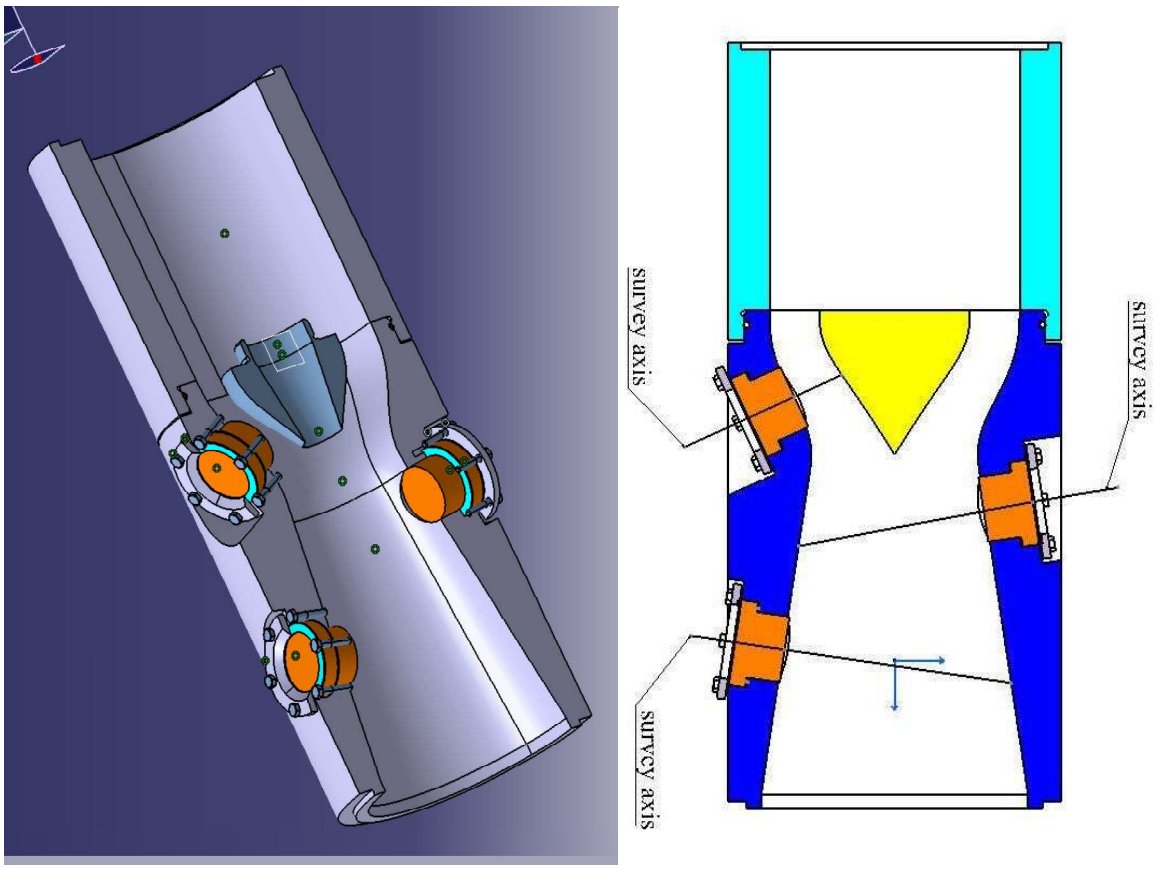

Fig. 8: Test section design.

The convergent-divergent test section, **Fig. 8**, has three windows for visualization of the velocity. The first window is located at 70 mm from the beginning of the convergent part, second window is located at 120 mm and third window at 200 mm. The axes of these windows are oriented along the local normal to the duct wall, for a minimum disturbance of the flow. The manufactured test section is shown in **Fig. 9**.

Fig. 9: Actual convergent-divergent test section manufactured from plexiglass.

The nozzle is manufactured from aluminium, in two versions shown in **Fig. 10**. One version has the full shape ending in the axis, while the other has a central hole for injecting the control jet.

Fig. 10: Central body manufactured without and with nozzle for control jet.

Velocity measurements are performed using a DANTEC Laser Doppler Velocimeter for two velocity components. The LDV system has a Spectra Physics air colled Laser with output power of 300 mW, and a 2D probe, 60 mm in diameter, 2.2 mm beam diameter, and focal length 160 mm. Two pairs of beams with wavelength of 488 nm and 514.5 nm are generated, and the probe includes a photomultiplier with

incorporated amplified. A 3D traversing system is used for probe positioning within a 0.01 mm accuracy on each axis. **Fig. 11** shows the actual LDV setup for one optical window.

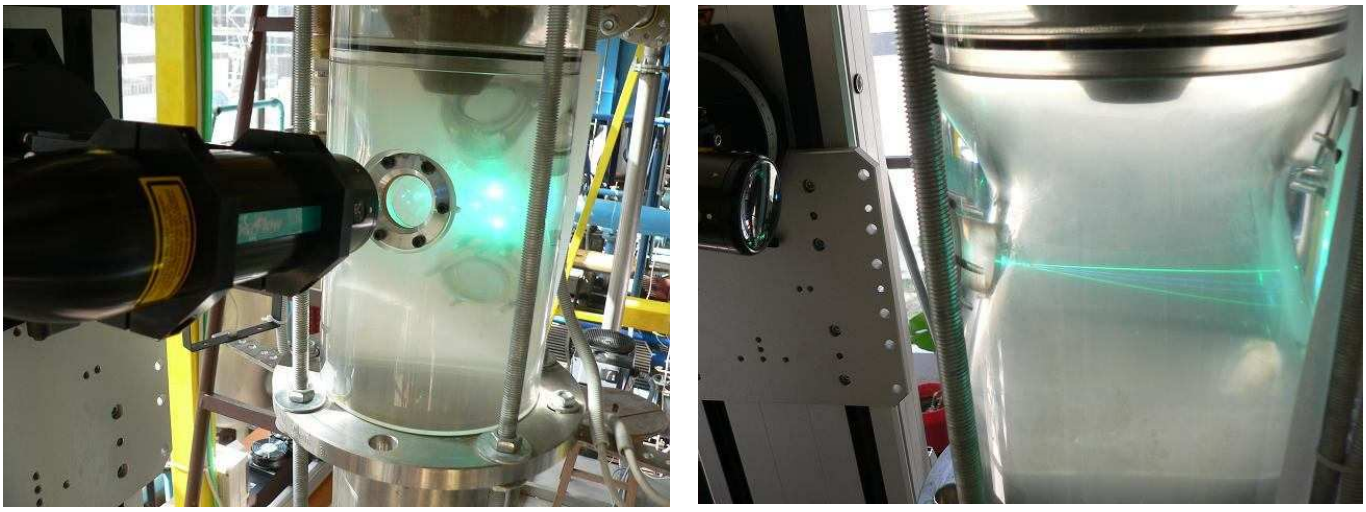

Fig. 11: LDV system for two-component velocity measurements.

A first example of meridian and circumferential velocity measurements is shown in **Fig. 12**. Each measured point follows the statistical analysis of up to 5000 measurements. The red lines correspond to the meridian velocity, while the green lines show the circumferential velocity component.

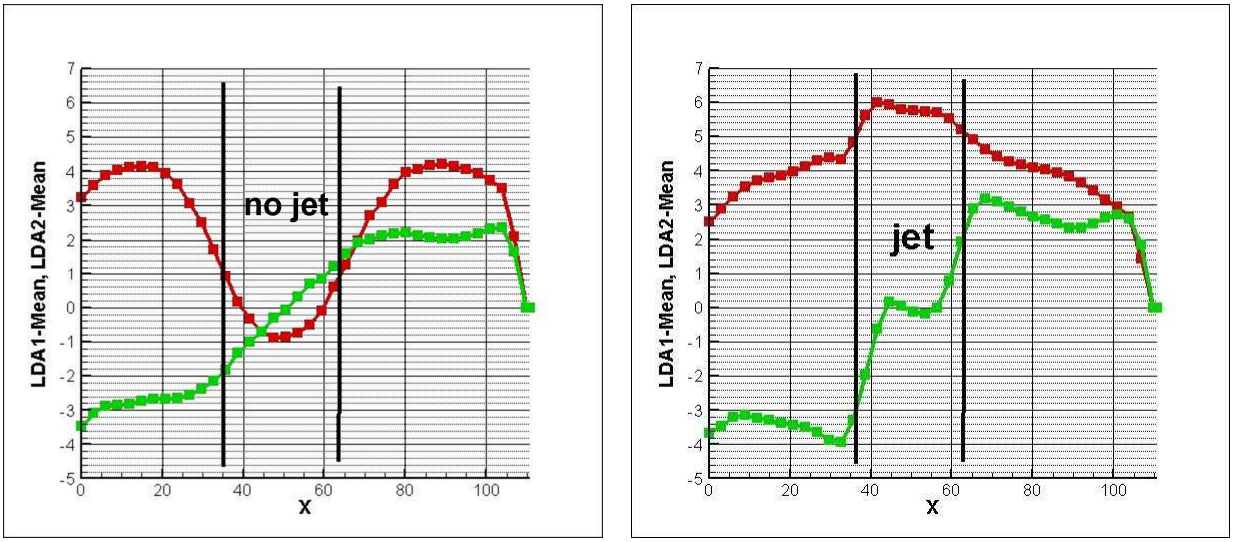

Fig. 12: Velocity profiles without (left) and with (right) control jet.

One can see from **Fig. 12** that without the jet we have a severe velocity deficit in the central region. When the control jet is on, we can achieve a meridian velocity profile simular to the one in a pipe. As far as the circumferential velocity is concerned, when we do not have the jet the central region rotates like a solid body. Once the jet is on, the circumferential velocity vanishes in a small region close to the axis, and increases sharply to the value in the main flow. Actually, the circumferential velocity becomes

locally larger than the corresponding values without due to the jet entrainment phenomenon which brings the streamtubes closer to the axis.

Conclusions

The paper presents the design of a convergent-divergent test section for the swirling flow apparatus developed at the “Politehnica” University of Timisoara – National Center for Engineering of Systems with Complex Fluids. For the convergent part we design a profiled shape of the duct wall and the central nozzle, using a methodology inspired from the wind tunnel contraction. We present the technical design and manufacturing details, as well as the experimental setup for LDV investigations of the meridian and circumferentail velocity components. Preliminary measurements of the velocity components are also shown, without and with control jet.

Acknowledgements

The present research has been supported by the Romanian National Authority for Scientific Research through the CEEX-C2-M1-1185 (C64/2006) “iSMART-flow” project, and by the Swiss National Science Foundation through the SCOPES Joint Research Project IB7320-110942/1.

References

[1] Bell, J.H., and Mehta, R.D.: “Transformation of a Polynomial Speed Wind Tunnels”, NASA CR 177488, 1998.

[2] Brassard, D., and Ferchichi, M.: “Transformation of a Polynomial for a Contraction Wall Profile”, Journal of Fluids Engineering, Vol. 127, pp. 183-185, 2005.

[3] Doolan, C.J.: “Numerical Evaluation of Contemporary Low-Speed Wind Tunnel Contraction Designs”, Journal of Fluids Engineering, Vol. 129, pp. 1241-1244, 2007.

[4] Kurokawa, J., Kajigaya, A., Matusi, J., Imamura, H.: “Suppresion of Swirl in a Conical Diffuser by Use of J-Groove”, Proc. 20th IAHR Symposium on Hydraulic Machinery and Systems, Charlotte, North Carolina, U.S.A., paper DY-01, 2000.

[5] Ionescu, G.D.: “Teoria Diferentiala a Curbelor si Suprafetelor cu Aplicatii Tehnice”, Dacia Publshing House, Cluj-Napoca, 1984. (in Romanian).

[6] Ciocan, G.D., Iliescu, M.S., Vu, T.C., Nennemann, B., and Avellan, F.: “Experimental Study and Numerical Simulation of the FLINDT Draft Tube Rotating Vortex”, Journal of Fluids Engineering, Vol. 129, pp. 146-158, 2007.

[7] Riley, K.F., Hobson, M.P., and Bence, S.J., Mathematical Methods for Physics and Engineering, Cambridge University Press, 1997.

[8] Susan-Resiga, R., Muntean, S., Bosioc, A., Stuparu, A., Miloş, T., Baya, A., Bernad, S., and Anton, L.E.: “Swirling Flow Apparatus and Test Rig for Flow Control in Hydraulic Turbines Discharge Cone”, Proceedings 2nd IAHR International Meeting of the Workgroup on Cavitation and Dynamic Problems in Hydraulic Machinery and Systems, Timişoara, Romania, Scientific Bulletin of the “Politehnica” University of Timişoara, Transactions on Mechanics, Tom 52(66), Fasc. 6, pp. 203-216, 2007.